AIAA 80-1559R

Predicted Vortex Shedding from Noncircular Bodies in Supersonic Flow

Michael R. Mendenhall*
Nielsen Engineering & Research, Inc., Mountain View, Calif.

A method to predict nose vortex shedding from circular and noncircular slender bodies in supersonic flow at angles of attack and roll is presented. The body is represented by a supersonic panel method, and the lee side vortex wake is modeled by discrete vortices in cross-flow planes. The three-dimensional steady flow problem is reduced to a two-dimensional, unsteady, separated flow problem for solution. Comparison of measured and predicted surface pressure distributions, flowfield surveys, and aerodynamic characteristics are presented for circular and elliptic bodies. Good agreement between experiment and theory for a range of flow conditions indicate that the principal features of the flow phenomena are modeled correctly.

Nomenclature

a = semimajor axis of elliptic cross section
A_l, B_l = coefficients of conformal transformation
b = semiminor axis of elliptic cross section
c_n = normal force coefficient per unit length
C_m = pitching moment coefficient
C_p = pressure coefficient
C_{p_I} = incompressible pressure coefficient
C_N = normal force coefficient
D = diameter of circular body, or equivalent diameter of noncircular body
l_{ref} = reference length, base diameter
L = total number of Fourier coefficients used to describe transformation, also model length
M_∞ = freestream Mach number
p = local static pressure
p_∞ = freestream static pressure
q_∞ = freestream dynamic pressure, $\frac{1}{2}\rho V_\infty^2$
r_0 = radius of circle
Re = freestream unit Reynolds number
S = reference area, $\pi D^2/4$
t = time
u_r = axial perturbation velocity
u_e = surface velocity in cross-flow plane
U = local velocity
v, w = velocity components in real plane
v' = velocity induced by a point vortex
V_∞ = freestream velocity
W = complex potential
x, y, z = body coordinate system with origin at the nose: x positive aft along the model axis, y positive to starboard, and z positive up
x_m = axial location of center of moments
α = angle of attack
α_c = angle between freestream velocity vector and body axis
β = angle of sideslip, also polar angle in σ-plane
γ = ratio of specific heats
Γ = vortex strength
δ = vortex reduction factor
Δt = time increment
Δx = axial length increment
θ = polar angle in ν-plane
ν = complex coordinate in real plane
ρ = freestream density
σ = complex coordinate in real plane
τ, λ = lateral and vertical coordinates in circle plane
ϕ = roll angle
Φ = velocity potential in real plane
ψ = stream function in real plane

Subscripts

$\bar{(\ )}$ = conjugate of complex quantity
e = boundary layer edge condition
m = vortex m

Introduction

THERE has been an increasing interest in missile applications requiring high aerodynamic performance and low radar cross section. These requirements can involve noncircular body shapes in supersonic flow at high angles of attack and nonzero roll angles. The angle of attack range may be sufficiently high to cause formation of body separation vortices. The vortex shedding characteristics are directly influenced by the body cross-sectional shape and the flow conditions; therefore, it is desirable to model the body vortex wake by means of a rational method capable of handling a variety of body shapes over a wide range of flow conditions.

The phenomena of interest are the sheets of vorticity formed on the lee side of a body at a high angle of attack. The vorticity is formed by boundary-layer fluid leaving the body surface from separation points on both sides of the body (Fig. 1) and rolling up into a symmetrical vortex pair. A method to predict these flow phenomena in the vicinity of circular and noncircular bodies in subsonic flow is described in Ref. 1.

The purpose of this paper is to describe an engineering method developed to predict the aerodynamic characteristics and associated flowfields of noncircular noses at high angles of attack in supersonic flow. The objectives of the method are to use a three-dimensional, attached flow, supersonic panel method to represent the body and a two-dimensional, incompressible, separated flow model to calculate the vortex shedding from the body alone at angle of attack and angle of roll. The predicted pressure distribution on the body under the influence of the freestream and the separation vortex wake will be used to calculate the aerodynamic loads on the body.

The following sections of this paper include a discussion of the approach to the problem and a description of the analysis and flow models required to carry out the calculation. The prediction method is evaluated through comparison of measured and predicted results on a variety of body shapes, including circular and elliptical cross sections.

Presented as Paper 80-1559 at the AIAA 7th Atmospheric Flight Mechanics Conference, Danvers, Mass., Aug. 11-13, 1980; submitted Oct. 14, 1980; revision received May 11, 1981.

*Manager, Engineering Fluid Mechanics Department. Member AIAA.

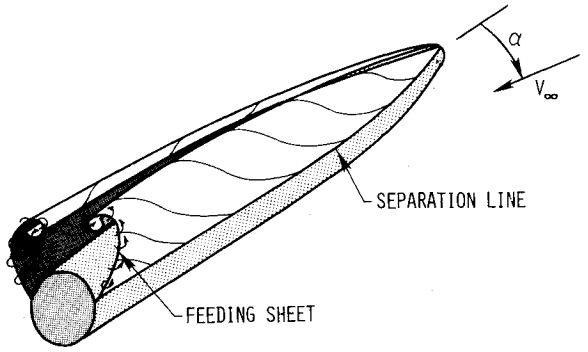

Fig. 1 Lee side vortex formation on an inclined body.

General Approach

Bodies at high angles of attack exhibit distributed vorticity fields on their lee side due to boundary-layer fluid leaving the body surface at separation lines. One approach to model these distributed vorticity fields has involved the use of clouds of discrete potential vortices. Underlying the basic approach is the analogy between two-dimensional unsteady flow past a body and the steady three-dimensional flow past an inclined body. In fact, the three-dimensional steady flow problem is reduced to the two-dimensional, unsteady, separated flow problem for solution. The details of the application of this approach to prediction of subsonic flow about circular and noncircular slender bodies are presented in Ref. 1. Other investigators have also used this approach to successfully model the subsonic flow phenomena in the vicinity of circular cross-sectional bodies.[2,3] The purpose of the work reported herein is to extend the previous subsonic analysis of Ref. 1 to supersonic flow.

The calculation procedure is carried out in the following manner. The body is represented by supersonic source panels, and the strength of the individual sources is determined to satisfy a flow tangency condition on the body in a non-separated uniform flow at angle of attack and roll. Starting at a cross-flow plane near the body nose, the pressure distribution on the body is computed using the full Bernoulli equation. The boundary layer in the cross-flow plane is examined for separation using the modified versions of Stratford's separation criteria. The Stratford's separation criteria are based on two-dimensional incompressible flow. At the predicted separation points, incompressible vortices with their strength determined by the vorticity transport in the boundary layer are shed into the flowfield. The trajectories of these free vortices between this cross-flow plane and the next plane downstream are calculated by integration of the equations of motion of each vortex, including the influence of the freestream, the body, and other vortices. At the next downstream cross-flow plane, new vortices are shed, adding to the vortex cloud representing the wake on the lee side of the body. This procedure is carried out in a stepwise fashion over the entire length of the body.

Methods of Analysis

The development of an engineering method to predict the pressure distributions on arbitrary missile bodies in supersonic flow at high angles of incidence requires the joining of several individual prediction methods. In this section, the individual methods are described briefly, and the section concludes with a description of the complete calculation procedure.

Noncircular Bodies

The cross-flow plane approach applied to arbitrary missile bodies results in a noncircular cross-sectional shape in the presence of a uniform cross-flow velocity and free vortices in each plane normal to the body axis. The procedure to handle the noncircular shapes is to find a conformal transformation

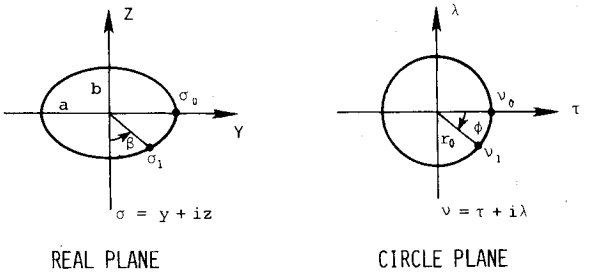

Fig. 2 Body cross-sectional nomenclature.

to map every point on or outside arbitrary body to a corresponding point on or outside a circular body. The two-dimensional potential flow solution around a circular shape in the presence of a uniform flow and external vortices is well known and has been documented numerous places in the literature.[2,4] Thus, the procedure is to obtain the potential solution for the circular body and transform it to the non-circular body.

For very simple shapes like an ellipse (Fig. 2), the transformation to the circle can be carried out analytically.[5] For example,

$$\sigma = \nu + \frac{a^2 - b^2}{4\nu} \tag{1}$$

where

$$\sigma = y + iz \tag{2}$$

in the real plane and

$$\nu = \tau + i\lambda \tag{3}$$

in the circle plane. The derivative of the transformation is

$$\frac{d\sigma}{d\nu} = 1 - \left(\frac{a^2 - b^2}{4\nu^2}\right) \tag{4}$$

which is required for the velocity transformation discussed later.

For complex noncircular shapes, the transformation cannot be carried out analytically and a numerical transformation is required. The numerical procedure chosen is a form of Theodorsen's transformation given by the relation

$$\frac{d\sigma}{d\nu} = \exp\left[\sum_{l=0}^{L} \frac{A_l - iB_l}{\nu^l}\right] \tag{5}$$

The coefficients, A_l and B_l are obtained from a numerical Fourier analysis procedure. Given the appropriate coefficients in Eq. (5), the mapping of known points in one plane to corresponding points in the second plane is carried out numerically as described in Appendix C of Ref. 6. The numerical mapping procedure is applicable to very general shapes given the coefficients of the transformation.

Body Panel Model

The configurations considered in this study are bodies alone, without fins or control surfaces. The body geometry is described by the coordinates of the cross-sectional shape at a number of axial stations, and linear interpolation between specific points is used. The body is represented by a three-dimensional lattice of supersonic source panels distributed on the surface of the body. The panels account simultaneously for volume and angle of incidence effects. The potential flow solution for a panel inclined to the flow direction is based on supersonic linear theory as described in Ref. 7 and the method used is a modified version of the program code presented in Ref. 8. In this approach, disturbances propagate along Mach

lines from points of origin on the body. The program was modified to account for combined angles of pitch and yaw, and specific modifications are described in detail in Ref. 9. The pitch and yaw angles are related to the included angle of attack and angle of roll by the expressions

$$\sin\alpha = \sin\alpha_c \cos\phi \tag{6}$$

$$\sin\beta = \sin\alpha_c \sin\phi \tag{7}$$

The flow tangency condition is applied at the control points of the body panels. Control points are located at the panel centroid. The result is a set of linear simultaneous equations in terms of unknown source panel strengths. Solution by an iterative approach produces the singularity strength on each panel and, thus, provides a means to calculate the velocity field induced by the body. The nature of the solution is such that the velocity on the body surface is correct only at the control points; therefore, linear interpolation is used to determine body surface velocity components at points lying between control points for use in pressure calculations.

There is a basic limitation in the use of the above panel method. The angle of inclination between a body source panel and the body centerline is limited to the semiapex angle of the Mach cone associated with the freestream Mach number. Thus, there is a limit to the body nose configurations which can be modeled by the body source panel method.

It should be noted here that the choice of the supersonic panel method to represent the body was dictated by the noncircular body requirement. Panel methods require large numbers of panels to obtain adequate detail in the flowfield, and as a consequence they contribute a large amount to the computational expense. If the bodies of interest were always circular in cross section, a better choice for the body model is the line singularity method described in Ref. 9.

Vortex Shedding Model

The vortex shedding model described in this section is nearly the same as the subsonic model presented in Ref. 1; therefore, the following description will be brief, and only the differences between the two models will be discussed in detail.

Equations of Motion

The equations of motion of a shed nose vortex in the presence of other free vortices in the vicinity of a body in a uniform stream follow. In the circle (ν) plane, the position of a vortex, Γ_m, is

$$\nu_{m_\Gamma} = \tau_m + i\lambda_m \tag{8}$$

and the image of Γ_m is located at

$$\nu_{m_{-\Gamma}} = \frac{r_0^2}{\bar{\nu}_m} \tag{9}$$

In the real plane, the position of the vortex Γ_m is

$$\sigma_{m_\Gamma} = y_m + iz_m \tag{10}$$

The complex potential in the real plane is

$$W(\sigma) = \Phi + i\Psi \tag{11}$$

and the corresponding velocity at Γ_m is

$$v_m - iw_m = \frac{dW_m(\sigma)}{d\sigma} = \frac{d}{d\nu}[W_m(\sigma)]\frac{d\nu}{d\sigma}\bigg|_{\substack{\sigma=\sigma_m \\ \nu=\nu_m}} \tag{12}$$

The complex potential of Γ_m is not included in Eq. (12) to avoid the singularity at that point. The derivative of the transformation is obtained from Eqs. (4) and (5).

The total velocity at Γ_m in the cross-flow plane is written as

$$\frac{v_m - iw_m}{V_\infty} = G_\alpha + G_\beta + G_n + G_m + G_T + G_r \tag{13}$$

where each term represents a specific velocity component in the σ-plane. The first term represents the uniform flow due to angle of attack.

$$G_\alpha = -i\sin\alpha\left[1 + \left(\frac{r_0}{\nu_m}\right)^2\right]\frac{d\nu}{d\sigma}\bigg|_{\sigma=\sigma_m} \tag{14}$$

The second term represents the uniform flow due to angle of yaw.

$$G_\beta = -\sin\beta\left[1 - \left(\frac{r_0}{\nu_m}\right)^2\right]\frac{d\nu}{d\sigma}\bigg|_{\sigma=\sigma_m} \tag{15}$$

The next term represents the influence of all vortices and their images, with the exception of Γ_m.

$$G_n = i\sum_{n=1}^{N}\frac{\Gamma_n}{2\pi r_0 V_\infty}\left[\frac{1}{(\nu_m/r_0) - (r_0/\bar{\nu}_n)} - \frac{1}{(\nu_m/r_0) - (\nu_n/r_0)}\right]_{n\neq m}\frac{d\nu}{d\sigma}\bigg|_{\sigma=\sigma_m} \tag{16}$$

The next term is due to the image of Γ_m.

$$G_m = i\frac{\Gamma_m}{2\pi r_0 V_\infty}\left[\frac{1}{(\nu_m/r_0) - (r_0/\bar{\nu}_m)}\right]\frac{d\nu}{d\sigma}\bigg|_{\sigma=\sigma_m} \tag{17}$$

The fifth term in Eq. (13) represents the potential of Γ_m in the σ-plane and is written as

$$G_T = -\frac{\Gamma_m}{2\pi V_\infty}\left(\frac{1}{2}\right)\frac{d}{d\nu}\left(\frac{d\nu}{d\sigma}\right)_{\sigma=\sigma_m} \tag{18}$$

The last term in Eq. (13) represents the velocity components induced by the portion of the body panel singularities representing the body volume effects.

$$G_r = \frac{v_r - iw_r}{V_\infty} \tag{19}$$

Since the body panel singularities are three dimensional, they contribute an induced axial velocity, u_r.

The differential equations of motion for Γ_m are

$$\frac{d\bar{\sigma}_m}{dx} = \frac{v_m - iw_m}{V_\infty\cos\alpha_c + u_r} \tag{20}$$

where

$$\bar{\sigma}_m = y_m - iz_m \tag{21}$$

Therefore, the two equations which must be integrated along the body length to determine the trajectory of Γ_m are

$$\frac{dy_m}{dx} = \frac{v_m}{V_\infty\cos\alpha_c + u_r} \tag{22}$$

and

$$\frac{dz_m}{dx} = \frac{w_m}{V_\infty\cos\alpha_c + u_r} \tag{23}$$

There are a pair of equations like Eqs. (22) and (23) for each vortex in the field. As new vortices are shed, the total number of equations to solve increases by two for each added vortex.

These differential equations are solved numerically using a method which automatically adjusts the step size to provide the specified accuracy.

Surface Pressure Distribution

The surface pressure distribution on the body is required to calculate the forces on the body and the separation points. The surface pressure coefficient is determined from the Bernoulli equation in the form

$$C_p = \frac{2}{\gamma M_\infty^2}\left\{\left[1+\frac{\gamma-1}{2}M_\infty^2(C_{p_I})\right]^{\gamma/(\gamma-1)}-1\right\} \tag{24}$$

where

$$C_p = \frac{p-p_\infty}{\frac{1}{2}\rho V_\infty^2} \tag{25}$$

and

$$C_{p_I} = 1-\left(\frac{U}{V_\infty}\right)^2 - \frac{2}{V_\infty^2}\frac{\mathrm{d}\phi}{\mathrm{d}t}\bigg|_{r_0} \tag{26}$$

In Eq. (26), U is the total velocity (including V_∞) at a point on the body. It consists of many of the components described in the previous section. The body-induced velocity components from Eq. (19) include the total effect of the panel solution at angle of attack and roll. As a consequence of using the full panel solution in this component, the two-dimensional doublet part of Eqs. (14) and (15) are not required. The vortex wake contribution is included through Eqs. (16) and (17). The last term in Eq. (26) represents the axial velocity induced by the two-dimensional singularities in the flow model. In this case, the shed vortices are the only singularities contributing to this term. Details of the calculation of this unsteady two-dimensional term are in Ref. 6.

Separated Wake

The separated wake on the lee side of the body is made up of a large number of discrete vortices, one shed from the separation points on either side of the body at each time step. The mechanics of the calculation of the individual vortices follow.

As described in Ref. 1, the pressure distribution in the cross-flow plane is referenced to the conditions at the minimum pressure point, and a virtual origin for the beginning of the boundary layer is assumed. The adverse pressure distribution downstream of the minimum pressure point is considered with either Stratford's laminar or turbulent separation criterion to determine whether or not separation has occurred. These criteria, based on two-dimensional, incompressible flat plate data, are adjusted for three-dimensional cross-flow effects in Ref. 1. Based on the compressibility limitations of the separation criteria, it is recommended that the cross-flow Mach number not exceed unity.

If the criteria indicate a separation point, the vorticity flux across the boundary layer at separation is shed into a single point vortex whose strength is

$$\frac{\Gamma}{V_\infty} = \frac{u_e^2}{2V_\infty^2}\frac{\Delta x}{\cos\alpha_c}\delta \tag{27}$$

assuming no slip at the wall. The empirical vortex strength reduction factor, δ, is widely used for subsonic flow to provide better agreement between measured and predicted vorticity in the wake. The factor is typically in the range of $0.6 \le \delta \le 1.0$ for subsonic flow.[2] The indication in supersonic flow is that $\delta \simeq 1.0$; therefore, in the present investigation, the vortex reduction factor is fixed at 1.0 unless otherwise noted.

The initial position of the shed vortex is determined such that the surface velocity at the separation point is exactly canceled by the shed vortex and its image. When this criterion results in a vortex initial position that is too near to the body surface, certain numerical problems cause difficulty in calculating the trajectory of this vortex. If this occurs, the vortex is arbitrarily placed at a point outside the boundary layer which is approximately 5% of the equivalent radius of the body.

Forces and Moments

The forces and moments on the body are computed by integration of the pressure distribution around the body. At a specified station on the body, the normal force coefficient on a Δx length of the body is

$$c_n = \frac{(\Delta n/\Delta x)}{q_\infty D} \tag{28}$$

The total normal force coefficient on the body is

$$C_N = \frac{N}{q_\infty S} = \frac{D}{S}\int_0^L c_n \mathrm{d}x \tag{29}$$

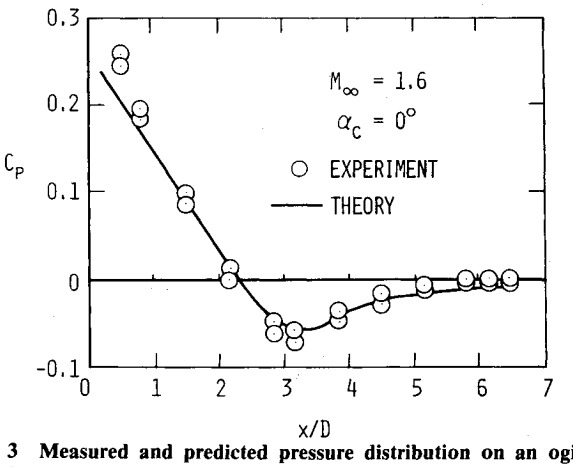

Fig. 3 Measured and predicted pressure distribution on an ogive cylinder, $\alpha = 0$ deg.

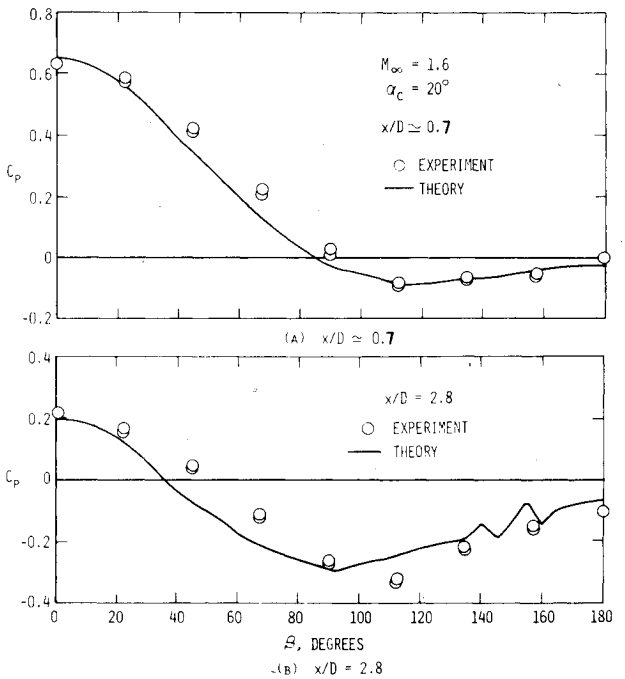

Fig. 4 Measured and predicted pressure distribution on an ogive cylinder, $\alpha = 20$ deg.

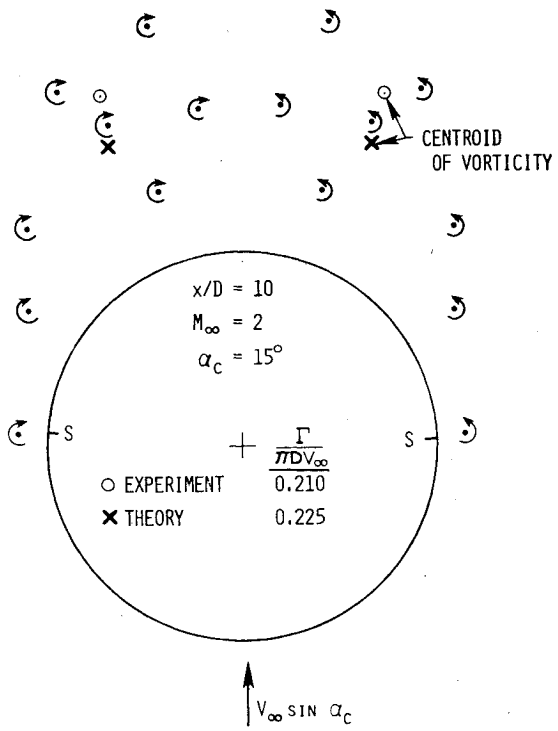

Fig. 5 Predicted vortex wake on the lee side of an ogive cylinder.

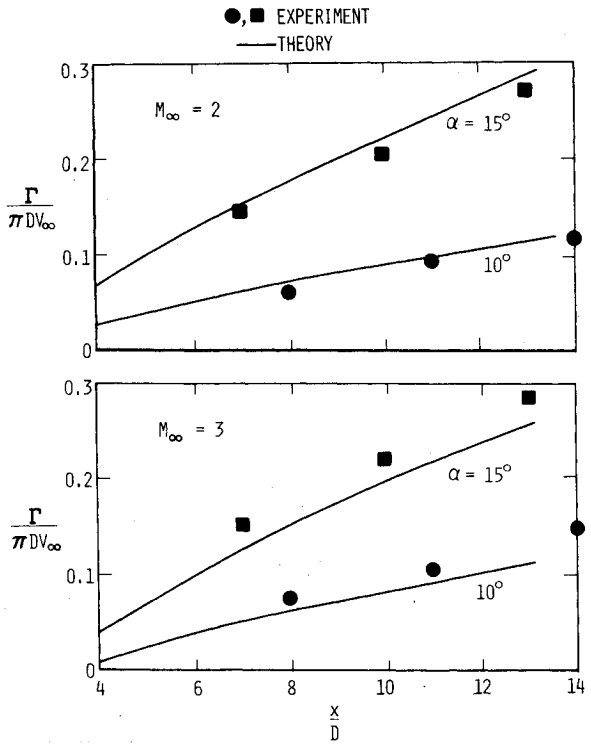

Fig. 6 Measured and predicted body vortex strength on the lee side of an ogive cylinder.

and the pitching moment coefficient is

$$C_m = \frac{M}{q_\infty S l_{ref}} = \frac{D}{S}\int_0^L c_n \left(\frac{x_m - x}{l_{ref}}\right) dx \qquad (30)$$

Similar expressions can be written for the side force and yawing moment coefficients.

Results

For purposes of evaluating the accuracy and range of applicability of the engineering prediction method described above, comparisons of measured and predicted aerodynamic

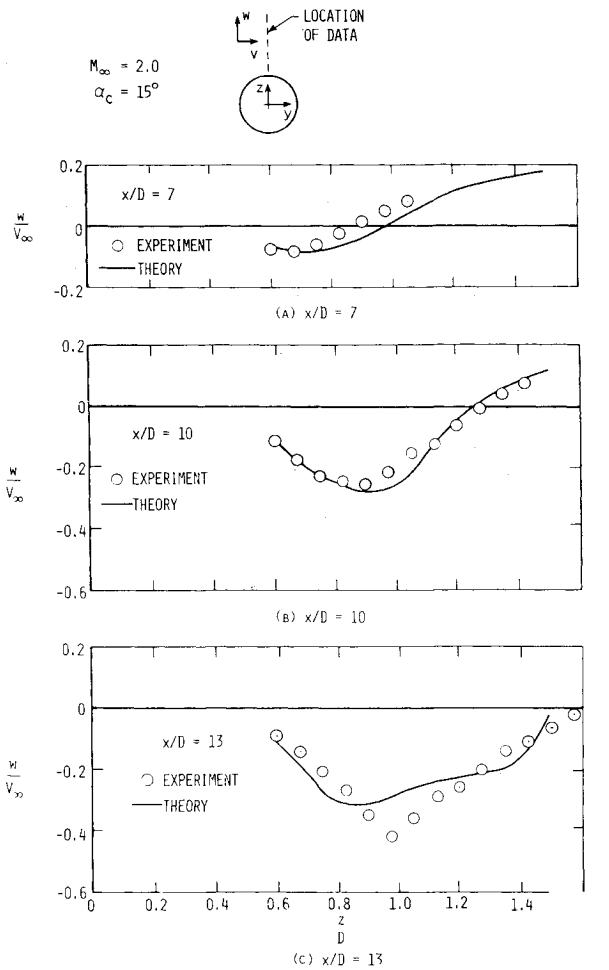

Fig. 7 Measured and predicted downwash distribution on the lee side of an ogive cylinder at $x/D = 7$, 10, and 13 deg.

characteristics of various configurations have been made. The objective of the method is to predict the characteristics for noncircular cross-sectional bodies, but most data available are for bodies of revolution. Circular cross-sectional bodies will be used to illustrate certain features of the prediction method. Some limited data on an elliptic cross section are available and these results are shown also. Typical results from the prediction method are presented in the following sections. Approximate execution time on a CDC-CYBER 175 is noted for several cases.

Circular Bodies

The prediction method was applied to an inclined ogive-cylinder model[10] in supersonic flow at high angles of attack to evaluate the ability of the prediction method to calculate pressure distributions. The configuration has a circular cross section and a three caliber ogive nose followed by a three and one-half caliber cylindrical afterbody. Circumferential pressure distributions at a large number of axial stations are available for a range of angles of attack and supersonic Mach numbers. The results to follow are all at $M_\infty = 1.6$ and a freestream Reynolds number, based on diameter, of 0.5×10^6.

The model was represented by 13 rings of 14 equally spaced circumferential panels for the calculation at $\alpha = 0$ deg (run time ≈ 10 s). The measured and predicted pressure distributions are compared in Fig. 3 where the multiple data symbols at each axial station represent the range of scatter in the data. The purpose of this comparison is to verify the paneling method and the pressure calculation technique under conditions in which there are neither cross-flow nor separation effects. The agreement is very good except in the

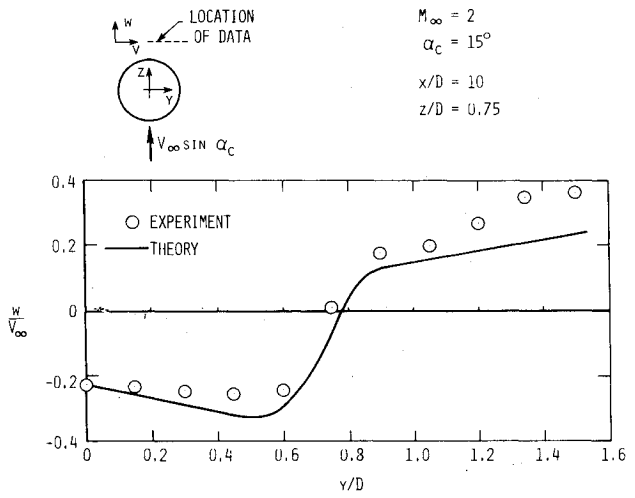

Fig. 8 Measured and predicted downwash distribution on the lee side of an ogive cylinder at $x/D = 10$ deg.

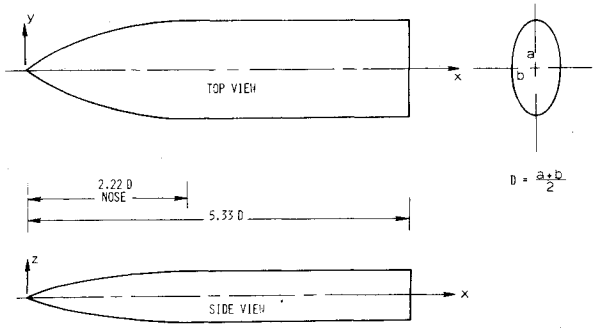

Fig. 9 The 2:1 elliptic cross-sectional body.

region very near the nose. It is possible that a finer grid of panels in this region would improve these results; however, for purposes of this investigation, a small error in the pressure very near the nose will have very little effect on the vortex shedding from the remainder of the body.

The prediction method was next applied to the same model at $\alpha = 20$-deg angle of attack (run time ≈ 100 s). At this angle of incidence, the separation vortex wake on the lee side of the body is well developed. Measured and predicted pressure distributions at two axial stations on the nose are compared in Fig. 4. The agreement between experiment and theory at $x/D \approx 0.7$, Fig. 4a, is very good except on the windward side of the body upstream of the minimum pressure point. Similar results are illustrated in Fig. 4b for a station near the end of the nose. The predicted minimum pressure point is upstream of the measured value, but the general trend of the predicted pressure distribution is correct. The irregular behavior of the predicted curve near $\beta = 140$ deg is caused by local interference of the lee side separation vortices.

The prediction method was next applied to an ogive-cylinder model for which detailed lee side flowfield measurements are available.[11] This model is an ogive-cylinder with a two caliber nose and a thirteen caliber cylindrical afterbody. The tests were conducted an Mach numbers of 2 and 3 at a freestream Reynolds number, based on diameter, of approximately 2×10^6. The data consists of lee side velocity components and separation vortex strengths and positions. Neither pressure nor force and moment data are available from these tests.

The model was represented by 15 rings of 14 equally spaced circumferential panels. The predicted vortex cloud pattern at $x/D = 10$ is shown in Fig. 5 for $M_\infty = 2$ and $\alpha = 15$ deg (run time ≈ 80 s). The vortex shedding is symmetric on both sides of the body. Also shown in this figure are the separation

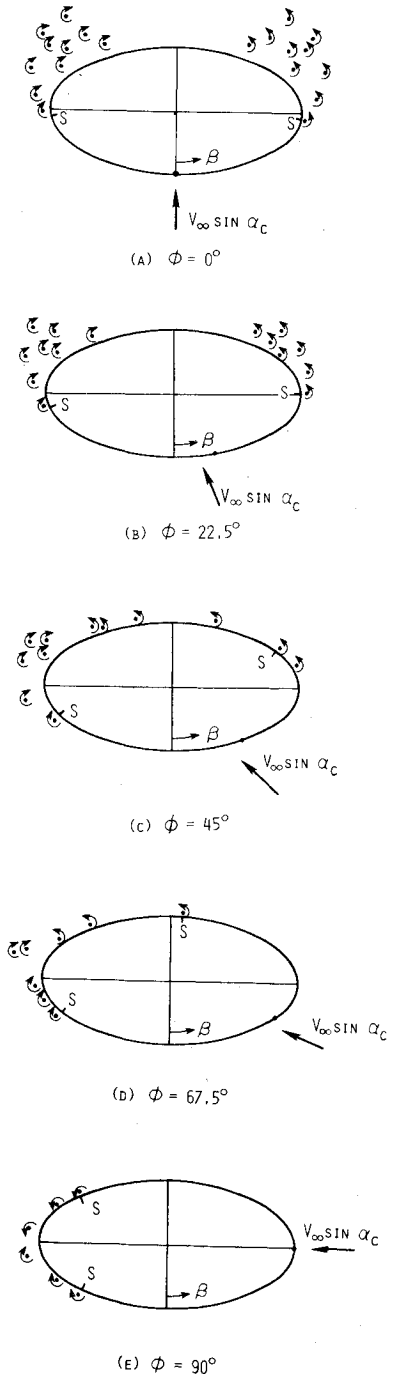

Fig. 10 Predicted vortex wake on an elliptic cross-sectional body at $x/D = 3.5$, $M_\infty = 1.5$, $\alpha_c = 15$ deg.

points located at approximately 93 deg measured from the windward stagnation point. The measured and predicted vortex strength and centroid of vorticity are shown to be in good agreement in this figure. The predicted vortex wake is approximately 7% stronger than the measured value, and the centroid of the predicted vortex cloud is slightly lower and more inboard than the measured results.

Measured and predicted body vortex strength on the ogive cylinder at Mach numbers 2 and 3 and angles of attack 10 and 15 deg are compared in Fig. 6. At $M_\infty = 3$, the predicted results are lower than those measured at both angles of attack. The slopes of the predicted curves are in good agreement with the experimental results, an indication that the predicted shedding rate and strengths of the shed vortices are correct. The difference in magnitude between the measured and predicted vortex strength in Fig. 6 is attributable to the location of the onset of separation. If separation is predicted

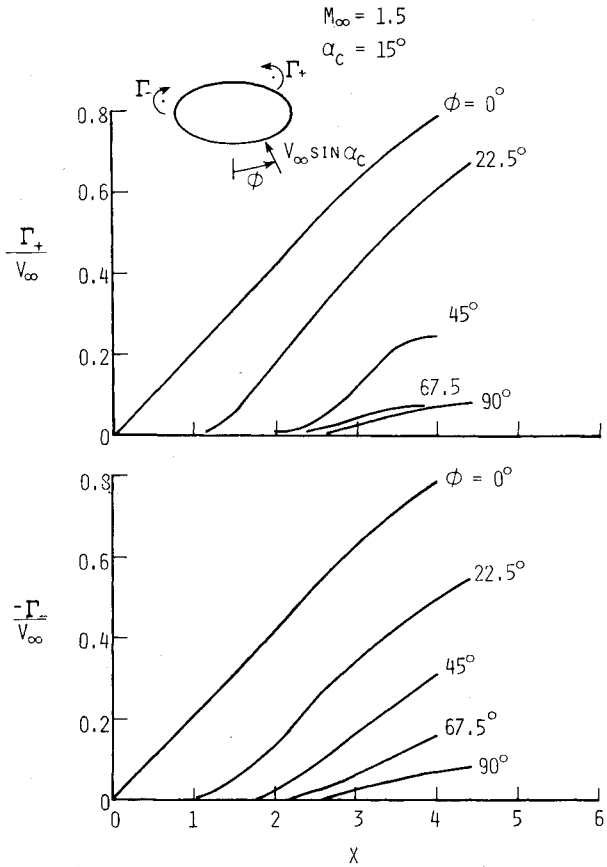

Fig. 11 Predicted body vortex strength on an elliptic cross-sectional body.

to start further aft on the body than the actual start of separation, the predicted vortex strength will be less than that measured. The maximum error in vortex strength exhibited in Fig. 6 represents an error in the predicted axial position of onset of separation of less than one body radius.

Measured and predicted downwash velocity fields in the plane of symmetry of the model are shown in Fig. 7 for three axial stations. The results are generally in good agreement, and the predicted velocity distribution exhibits the correct trend in every case. The measured and predicted downwash velocities along a horizontal line through the center of the vortex wake are shown in Fig. 8. These results are also in good agreement.

Elliptic Bodies

The prediction method has been applied to the elliptic cross-sectional body shown in Fig. 9. The major axis of the cross section is specified by an ogive distribution on the nose, and the cross section is a 2:1 ellipse over the entire body length. The equivalent base diameter of this body is 1.125 in. Circumferential pressure measurements at numerous axial stations are available at $M_\infty = 1.5$ and a range of angles of incidence and angles of roll. The tests were conducted at a freestream Reynolds number, based on the equivalent diameter, of approximately 0.3×10^6.

The predicted vortex cloud patterns on the elliptic body at approximately 3.5 equivalent base diameters from the nose ($x = 4$ in.) are shown in Fig. 10. The conditions represented in this figure are $M_\infty = 1.5$, $\alpha_c = 15$ deg, and a range of roll angles from 0 to 90 deg. At $\phi = 0$ deg, the separated wake is symmetric about the plane of symmetry, but as the body rolls, asymmetry in the wake begins to develop because of the different curvatures of the body to the right and left sides of the stagnation point (shown as a dot on the body in Fig. 10). The right and left separation points are denoted as S in this figure. Notice that the right side separation point remains

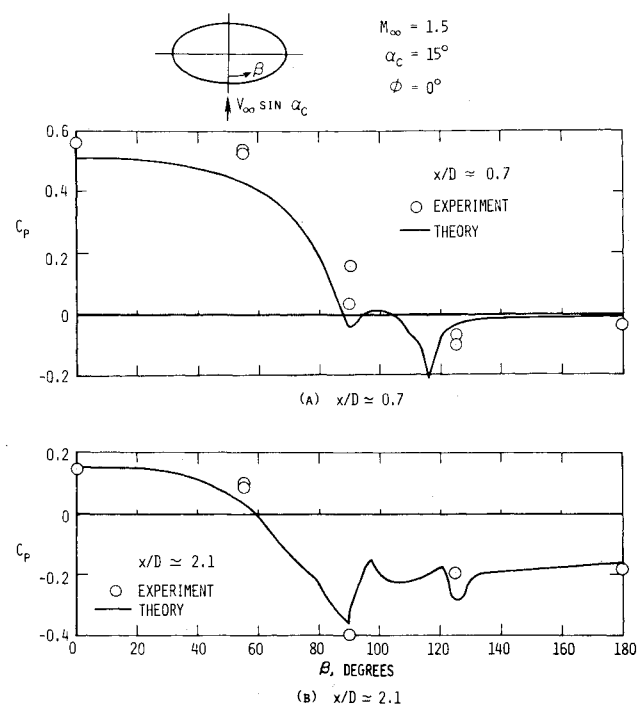

Fig. 12 Measured and predicted pressure distribution on an elliptic cross-sectional body, $\alpha_c = 15$ deg, $\phi = 0$ deg.

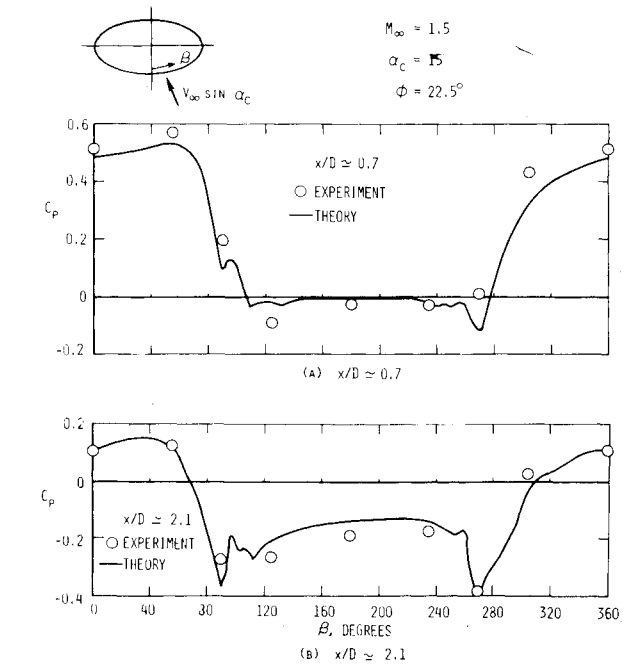

Fig. 13 Measured and predicted pressure distribution on an elliptic cross-sectional body, $\alpha_c = 15$ deg, $\phi = 22.5$ deg.

near $\beta = 90$ deg until a roll angle of greater than 45 deg, then it moves rapidly to approximately $\beta = 170$ deg at $\phi = 67.5$ deg. The left side separation point has a much smaller range of motion as the roll angle increases. At a roll angle of 90 deg, the flow is again symmetric.

The effect of roll angle on the strength of the right (Γ_+) and left (Γ_-) side separation vortices is shown in Fig. 11. Comparison of corresponding curves in the top and bottom portions of this figure serves to illustrate the different growth patterns of the right and left vortices. Note that at $\phi = 45$ deg, separation begins closer to the nose on the left side of the body than on the right side, and the left vortex grows in strength more rapidly initially than does the right.

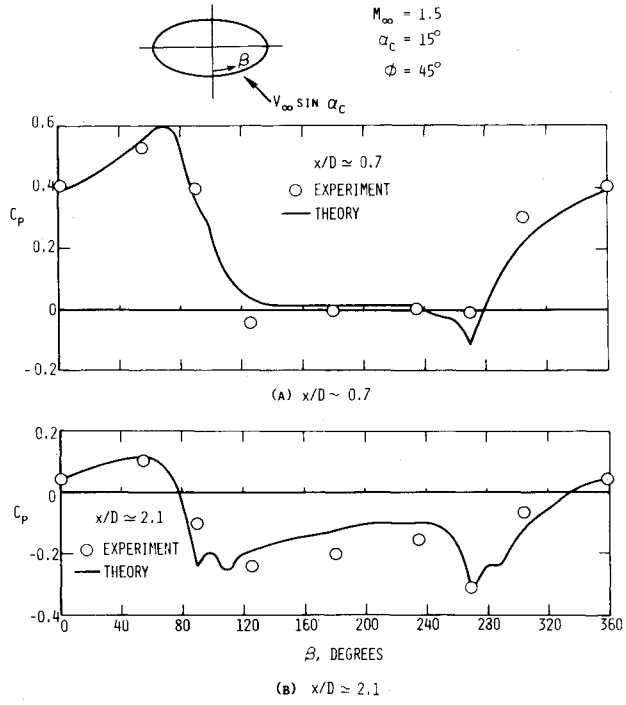

Fig. 14 Measured and predicted pressure distribution on an elliptic cross-sectional body, $\alpha_c = 15$ deg, $\phi = 45$ deg.

Measured and predicted pressure distributions on the elliptic cross-sectional body at $M_\infty = 1.5$, $\alpha_c = 15$ deg, and $\phi = 0$ deg are compared in Fig. 12 at two axial stations on the nose (run time ≈ 70 s). The agreement between experiment and theory is better away from the nose. The sparse nature of the measurements make it difficult to fully evaluate the prediction method other than to observe that the basic trends of the pressure distribution are predicted. At $x/D \approx 2.1$, the separation vorticity has grown in strength and scope, and the major region of vortex wake influence covers the region between $\beta = 90$ and 130 deg.

The predicted pressure distributions on the same body at roll angles of 22.5 and 45 deg are shown in Figs. 13 and 14, respectively (run time ≈ 200 s). The predicted results are generally in good agreement with experiment, and the correct trends of the data are modeled by the theory in each case. The local irregularities in the predicted curves are due to the influences of the separation vortices.

Conclusions

An engineering method to predict the vortex shedding from circular and noncircular slender bodies in supersonic flow at angles of attack and roll is described. The coupling of a supersonic panel method and a two-dimensional cross-flow method has proved to be a successful means to predict the general flow characteristics about slender, circular, and noncircular bodies at large angles of incidence. Comparisons of measured and predicted pressure distributions and associated flowfields on a variety of bodies indicate that the principal features of the flow phenomena are modeled. The predicted vorticity distributions in the wake of a body of revolution in supersonic flow are in good agreement with experiment. This also results in good agreement between measured and predicted velocity components in the flowfield of the body. The ability to predict the vortex wake-induced velocities with some accuracy provides an important capability. The ability to model the correct flowfield near the body leads to the calculation of wake-induced interference effects on fins and other control surfaces as well as surface pressure distributions. The vortex shedding analysis described herein can be incorporated into an overall computation method for missiles and aircraft. Preliminary work in this area is reported in Ref. 13.

Acknowledgment

The work reported herein was sponsored by the NASA Langley Research Center under Contract NAS1-15931.

References

[1] Mendenhall, M.R., Spangler, S.B., and Perkins, S.C. Jr., "Vortex Shedding from Circular and Noncircular Bodies at High Angles of Attack," AIAA Paper 79-0026, Jan. 1979.

[2] Marshall, F.J. and Deffenbaugh, F.D., "Separated Flow over Bodies of Revolution Using an Unsteady Discrete-Vorticity Cross Wake," NASA CR-2414, June 1974.

[3] Deffenbaugh, F.D. and Koerner, W.G., "Asymmetric Wake Development and Associated Side Force on Missiles at High Angles of Attack," AIAA Paper 76-364, July 1976.

[4] Mendenhall, M.R. and Nielsen, J.N., "Effect of Symmetrical Vortex Shedding on Longitudinal Aerodynamic Characteristics of Wing Body Combinations," NASA CR-2473, Jan. 1975.

[5] Nielsen, J.N., *Missile Aerodynamics,* McGraw-Hill Book Co., New York, 1960.

[6] Spangler, S.B. and Mendenhall, M.R., "Further Studies of Aerodynamic Loads at Spin Entry," Report ONR-CR215-225-3, June 1977.

[7] Woodward, F.A., "An Improved Method for the Aerodynamic Analysis of Wing-Body-Tail Configurations in Subsonic and Supersonic Flow. Part I—Theory and Application," NASA CR-2228, Part I, May 1973.

[8] Woodward, F.A., "An Improved Method for the Aerodynamic Analysis of Wing-Body-Tail Configurations in Subsonic and Supersonic Flow. Part II—Computer Program Description," NASA CR-2228, Part II, May 1973.

[9] Dillenius, M.F.E. and Nielsen, J.N., "Computer Programs for Calculating Pressure Distributions Including Vortex Effects on Supersonic Monoplane or Cruciform Wing-Body-Tail Combinations with Round or Elliptical Bodies," NASA CR-3122, April 1979.

[10] Landrum, E.J., "Wind-Tunnel Pressure Data at Mach Numbers from 1.6 to 4.63 for a Series of Bodies of Revolution at Angles of Attack from $-4°$ to 60°," NASA TM X-3558, Oct. 1977.

[11] Oberkampf, W.L. and Bartell, T.J., "Supersonic Flow Measurements in the Body Vortex Wake of an Ogive Nose Cylinder," AFATL-TR-127, Nov. 1978.

[12] Goodwin, F.K. and Dyer, C.L., "Data Report for an Extensive Store Separation Test Program Conducted at Supersonic Speeds," AFFDL-TR-79-3130, Dec. 1979.

[13] Smith, C.A. and Nielsen, J.N., "Prediction of Aerodynamic Characteristics of Cruciform Missiles to High Angles of Attack Utilizing a Distributed Vortex Wake," Nielsen Engineering and Research (NEAR) TR 208, Jan. 1980.